HHS Public Access

Author manuscript

Cell Rep. Author manuscript; available in PMC 2021 March 20.

Published in final edited form as:

Cell Rep. 2021 February 16; 34(7): 108752. doi:10.1016/j.celrep.2021.108752.

An mTORC1-dependent switch orchestrates the transition between mouse spermatogonial stem cells and clones of progenitor spermatogonia

Shinnosuke Suzuki[1], **John R. McCarrey**[1], **Brian P. Hermann**[1,2,*]

[1]Department of Biology, University of Texas at San Antonio, San Antonio, TX 78249, USA

[2]Lead contact

SUMMARY

Spermatogonial stem cells (SSCs) sustain spermatogenesis by balancing self-renewal and initiation of differentiation to produce progenitor spermatogonia committed to forming sperm. To define the regulatory logic among SSCs and progenitors, we performed single-cell RNA velocity analyses and validated results *in vivo*. A predominant quiescent SSC population spawns a small subset of cell-cycle-activated SSCs via mitogen-activated protein kinase (MAPK)/AKT signaling. Activated SSCs form early progenitors and mTORC1 inhibition drives activated SSC accumulation consistent with blockade to progenitor formation. Mechanistically, mTORC1 inhibition suppresses transcription among spermatogonia and specifically alters expression of insulin growth factor (IGF) signaling in early progenitors. *Tex14*$^{-/-}$ testes lacking intercellular bridges do not accumulate activated SSCs following mTORC1 inhibition, indicating that steady-state mTORC1 signaling drives activated SSCs to produce progenitor clones. These results are consistent with a model of SSC self-renewal dependent on interconversion between activated and quiescent SSCs, and mTORC1-dependent initiation of differentiation from SSCs to progenitor clones.

Graphical Abstract

*Correspondence: brian.hermann@utsa.edu.

AUTHOR CONTRIBUTIONS

Experiments were designed by S.S. and B.P.H.; data were collected and analyzed by S.S.; and interpretations, conclusions, and writing were by S.S., J.R.M., and B.P.H.

SUPPLEMENTAL INFORMATION

Supplemental Information can be found online at https://doi.org/10.1016/j.celrep.2021.108752.

DECLARATION OF INTERESTS

The authors declare no competing interests.

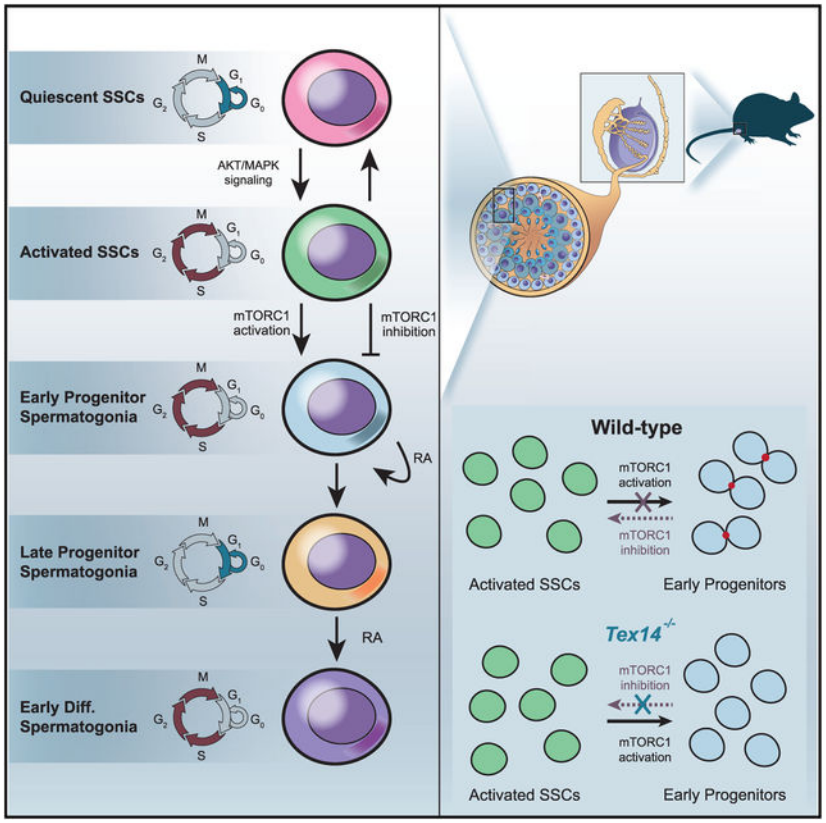

In Brief

Suzuki et al. define relationships between subsets of adult mouse SSCs and progenitor spermatogonia using single-cell RNA velocity analyses and *in vivo* validations. Quiescent SCCs convert to cell-cycle-activated SCCs via MAPK/AKT signaling. Activated SCCs are driven to become early progenitor clones ready to initiate differentiation through mTORC1 signaling.

INTRODUCTION

In the testis, spermatogenesis is anchored by spermatogonial stem cells (SSCs), which sustain a hierarchy of mitotic spermatogonia. Some spermatogonia respond to retinoic acid (RA), activate KIT proto-oncogene receptor tyrosine kinase (KIT) expression, and initiate differentiation (Busada et al., 2015a; de Rooij and Russell, 2000), whereas others persist as undifferentiated spermatogonia (Busada et al., 2015a; Endo et al., 2017; Ikami et al., 2015; Zhou et al., 2008). SSCs comprise a small subset of undifferentiated spermatogonia functionally distinguished by their ability to both self-renew perpetually and give rise to progenitor spermatogonia committed to producing sperm (Hara et al., 2014; Helsel et al., 2017b; Hermann et al., 2018; Ikami et al., 2015; Nakagawa et al., 2007, 2010).

Several models describing the relationship between SSCs and progenitors provide a framework for investigating mechanisms regulating SSC fate (Lord and Oatley, 2017). The traditional A_{single} model (de Rooij, 1969; Huckins, 1971; Oakberg, 1971) holds that SSCs are exclusively A_{single} spermatogonia, whereas $A_{paired/aligned}$ spermatogonia are progenitors

irreversibly committed to differentiation. This model implies homogeneity among A_{single} spermatogonia (de Rooij and Russell, 2000; Mutoji et al., 2016). An alternate fragmentation model holds that clones of undifferentiated spermatogonia can interconvert between A_{single} and $A_{paired/aligned}$ states (Hara et al., 2014; Nakagawa et al., 2007, 2010). A revised A_{single} model accommodates recent evidence of heterogeneity among undifferentiated spermatogonia (Lord and Oatley, 2017).

The advent of technologies to survey the entire mRNA transcriptome with single-cell resolution (single-cell RNA sequencing [scRNA-seq]) reveals transcriptome heterogeneity among otherwise homogeneous cells to resolve potential subtypes (Lafzi et al., 2018). Using scRNA-seq datasets from testicular germ cells, we and others ordered spermatogenic cells in pseudotime to distinguish cell states (e.g., SSC versus progenitor and subdivisions thereof) and to infer cell trajectories reflective of state transitions and the responsible regulatory framework (Cheng et al., 2020; Green et al., 2018; Hermann et al., 2018; La et al., 2018b; Li et al., 2017; Lukassen et al., 2018; Song et al., 2016; Suzuki et al., 2019). Although these analyses have uncovered many cell states and pathways, they are limited by computational assumptions and the static nature of steady-state mRNA levels. RNA velocity analysis exploits data arising from the nascent unspliced transcriptome embedded within scRNA-seq datasets empirically indicative of cell-state trajectories (La Manno et al., 2018; Svensson and Pachter, 2018). We have used RNA velocity analysis to identify two discrete transitions between mouse SSCs and progenitor spermatogonia: (1) an interconversion of SSCs between quiescent and activated cell-cycle states associated with changes to mitogen-activated protein kinase (MAPK) and phosphatidylinositol 3-kinase (PI3K)/AKT serine/threonine kinase (AKT) signaling and (2) an mammalian target of rapamycin complex 1 (mTORC1)-dependent switch between activated SSCs and clones of early progenitor spermatogonia influenced by RA. These results refine our understanding of the underlying molecular mechanisms driving SSC self-renewal or initiation of differentiation.

RESULTS

RNA velocity analysis of adult spermatogenesis

We first applied RNA velocity analysis to adult mouse spermatogenic cells at all phases of spermatogenic maturation from spermatogonia to spermatids (Hermann et al., 2018) and observed nearly exclusive unidirectional trajectory vectors along the spermatogenesis continuum (Figures S1A–S1C). This revealed spermatogenic phases bearing little transcriptional change interspersed with phases of significant transcriptomic flux (Figure S1C), including examples of genes that became transcriptionally active and enriched in the unspliced form in spermatogonia in advance of meiotic entry and their subsequent accumulation in the spliced mRNA form in spermatocytes (Figures S1D and S1E).

Distinct clusters of cell-cycle-activated and quiescent SSCs

We next performed focused analysis of adult ID4-EGFP^{Bright} spermatogonia known not only to be enriched for transplant-competent SSCs but also to contain progenitor spermatogonia and a small population of differentiating spermatogonia (Hermann et al., 2018) (Figures 1A–1C; Figures S1F–S1I; Table S1). This identified 14 cell clusters among ID4-EGFP^{Bright}

spermatogonia, with only clusters 1 and 7 designated as SSCs: high levels of SSC markers (*Dusp6*, *Eomes*, *Etv5*, *Gfra1*, and *Id4*) and low or absent detection of either progenitor markers (*Lin28a*, *Nanos3*, *Neurog3*, *Pou5f1*, *Rarg*, or *Sox3*) or canonical differentiation markers (*Kit* and *Stra8*) (Figures 1A–1C; Figures S1F–S1I; Table S1). Cells in clusters 2, 5, and 6 were designated progenitors, expressing progenitor markers (*Lin28a*, *Nanos3*, *Neurog3*, *Pou5f1*, *Rarg*, and *Sox3*) with little or no detection of either SSC markers (*Dusp6*, *Eomes*, *Etv5*, *Gfra1*, or *Id4*) or differentiation markers (*Kit* or *Stra8*). Cells in clusters 3, 9, and 11 reflect early differentiating spermatogonia, with high levels of differentiating markers (*Kit* and *Stra8*) and little or no detection of SSC markers (*Dusp6*, *Eomes*, *Etv5*, *Gfra1*, or *Id4*). Cells in the tiny clusters 13 and 14 were contaminating somatic cells (Figures 1A–1C; Figures S1F–S1I; Table S1). We resolved cluster 5 as early progenitors with lower levels of progenitor markers than those of the late progenitors in clusters 2 and 6 (Figures 1A–1C; Figures S1F–S1I; Table S1). Cells in clusters 4, 8, and 12 showed intermediate phenotypes, with hybrid SSC/progenitor transcriptomes, likely reflecting populations in flux (Figures 1A–1C; Figures S1F–S1I; Table S1). Cluster 1 consisted of 82.7% of SSCs with modest inward vectors suggesting maintenance of this state, whereas larger vectors in cluster 7 were directed outward toward both intermediate cluster 8 and SSC cluster 1 (Figure 1C; Figure S1F). Between the two SSC populations in clusters 1 and 7, we found only 18 genes upregulated in cluster 1, whereas 530 were upregulated in cluster 7 (Table S1). Gene Ontology (GO) analysis indicated cell-cycle activation in cluster 7 (Figure 1D; Figure S1J; Table S2). In all, a large proportion of cluster 7 SSCs, cluster 5 early progenitors, and cluster 3/9/11 differentiating spermatogonia were categorized as cell cycle active (G1/S, S, G2, or G2/M) (Figures 1E and 1F). Conversely, most cluster 1 SSCs and cluster 2/6 late progenitors were in the M/G1 category (Figures 1E and 1F), indicative of G0 arrest and quiescence (Figure S1J) (Lauridsen et al., 2018; Whitfield et al., 2002). Quiescent SSCs exhibited inward vectors, suggesting maintenance of this state, whereas activated SSCs showed outward vectors directed toward both quiescent SSCs and SSC/early progenitor intermediary populations (Figure 1C). We confirmed these sub-populations of SSCs and progenitors using data from PLZF-mCherry+/KIT− spermatogonia (La et al., 2018b) (Figure S2; Tables S1 and S2). Altogether, these results confirm distinct adult SSC and progenitor populations, with early progenitors arising from activated SSCs that interconvert with quiescent SSCs.

We then performed *in vivo* analyses using flow cytometry and whole-mount immunofluorescence. Using adult *Id4-Egfp* mice (Figures 2A–2D) or C57BL/6 mice (Figures S3A–S3E), we found that in agreement with the scRNA-seq results, 71.7% ± 0.32% of ID4-EGFP^{Bright}/SOX3^{low}/RARγ^{low} SSCs and 80.7% ± 1.92% of PLZF^{low}/SOX3^{low}/RARγ^{low} SSCs were quiescent (Ki67$^{low/-}$), whereas the remainder were proliferative (Ki67^{high}) (Figure 2D; Figure S3E). Both quiescent and active (Ki67^{high}) SSC populations were present throughout the cycle of the seminiferous epithelium, with the greatest level of Ki67 labeling among SSCs present in the late stages (X–XII) and the lowest level in the early stages (I–V) (Figures 2E–2H; Figure S3F). SSC Ki67-labeling indices were not significantly different by stage, excluding the possibility that prevalence of quiescent and active SSCs is linked to stage of the cycle of the seminiferous epithelium. Heterogeneous labeling for two progenitor markers, SOX3 and RARγ, matched mRNA expression patterns (Figures 1A–1C and 2B; Figures S1F–S1H, S3C, and S3G) characteristic of early

progenitors (PLZF^{low}/SOX3^{high}/RARγ^{low}) and late progenitors (PLZF^{high}/SOX3^{high}/RARγ^{high}), respectively. More early progenitors were Ki67+ than either SSCs or late progenitors (Figures S3E and S3G); thus, early progenitors are likely primary, transit-amplifying, undifferentiated spermatogonia.

Finally, we treated mice with either a bolus of RA or a 2-day treatment with WIN18,446 to inhibit RA signaling, which normally induces RARγ-expressing progenitors to differentiate (Feng et al., 2000; Ikami et al., 2015). As expected, RA reduced the proportion of PLZF^{high}/KIT^{neg} undifferentiated spermatogonia (Figures S4A–S4D), but it did not change the PLZF^{low}/KIT^{neg} population, indicating that PLZF^{low}/KIT^{neg} spermatogonia are enriched for SSCs. In addition, RA induced proliferation of RARγ^{high} late progenitors and their differentiation (becoming KIT+) and significantly enhanced the Ki67-labeling index in early progenitors and their overall proportion, whereas WIN18,446 impeded late progenitor proliferation and formation of KIT+/PLZF^{high}-differentiating spermatogonia (Figures S4A–S4F) and reduced early progenitor proliferation (Figure S4D). Because RARγ expression is, by definition, absent from early progenitors and present in late progenitors, these results indicate that RA can directly initiate the differentiation of late progenitors and indirectly drive early progenitor proliferation.

SSC and progenitor populations exhibit distinct signaling characteristics

We identified expression of 13 genes that were upregulated in cluster 7 relative to cluster 1 and are known to be activated by the glial cell line derived neurotrophic factor family receptor alpha 1 (GFRA1)/ret proto-oncogene(RET) pathway in cultures containing a mixture of SSCs and progenitors (Oatley et al., 2006) (*Ccne1*, *Ccne2*, *Chaf1b*, *Dnajb11*, *Gsta4*, *GtROSA26Sor*, *Mmd*, *Pcna*, *Pou3f1*, *Rbm12*, *Rrm2*, *Snrpa1*, and *Ube2a*) (Table S1), suggesting that activation of GFRA1/RET signaling triggers cell-cycle activation in SSCs. We then analyzed the phosphorylation levels of p44/42 MAPK, AKT (pan), and ribosomal protein S6 (RPS6), a downstream target of mTORC1 signaling, because GFRA1/RET signaling activates these pathways (La et al., 2018a; Wang et al., 2017). Compared with quiescent SSCs, activated SSCs and early progenitors showed significantly increased MAPK and AKT signaling, whereas enhanced activation of mTORC1 signaling was seen only in early progenitors (Figures 3A–3E). These results correlate active MAPK, PI3K/AKT, and mTORC1 signaling with a stepwise transition from quiescent SSCs, to activated SSCs, to early progenitors.

Based on the expression of cell-type-specific markers (Figure 1B) identifying cluster 5 as early progenitors, not SSCs, our RNA velocity data suggest that early progenitors (cluster 5) exist in an unstable state interconverting with SSCs (clusters 1 and 7) and late progenitors (clusters 2 and 6) (Figures 1A–1C; Figures S1F–S1I). Early progenitors in cluster 5 occupied a somewhat intermediate phenotype, with lower levels of SSC markers and higher levels of progenitor markers compared with SSCs (clusters 1 or 7) but lower levels of progenitor markers compared with late progenitors (clusters 2 or 6) (Figures 1A–1C; Figures S1F–S1I; Table S1). Because mTORC1 signaling was enhanced only in early progenitors (Figures 3C–3E) and mTORC1 inhibition increased the proportion of GFRA1-positive cells (Hobbs et al., 2010; La et al., 2018a), we hypothesized that mTORC1 signaling drives the

formation of early progenitors from activated SSCs. To test this hypothesis, we treated mice with rapamycin to inhibit mTORC1 (Hobbs et al., 2010; La et al., 2018a), as confirmed by significantly attenuated phosphorylated RPS6 (p-RPS6) levels (Figure 3F). Rapamycin significantly reduced the proportion of early progenitors and increased the proportion of activated SSCs but left late progenitors unchanged (Figures 3G and 3H), indicating that mTORC1 signaling is specifically involved in controlling the SSC-to-progenitor transition.

mTORC1 signaling regulates the balance between SSC self-renewal and commitment to differentiation

To interrogate the effects of mTORC1 signaling on gene expression and cell-type relationships among undifferentiated spermatogonia, we performed scRNA-seq using adult Id4-EGFP^{Bright} spermatogonia from (1) untreated mice (control), (2) mice treated with rapamycin for 2 days (rapamycin treated), and (3) mice treated with rapamycin for 2 days and then discontinued for 1 day (rapamycin release) (Figure 4A; Figures S5A and S5B). Two days of rapamycin treatment induced changes to the RNA velocity vectors among all populations, coinciding with activated SSC accumulation and early progenitor depletion (Figure 4I; Figures S5A, S5B, and S5M). Indeed, RNA velocity vectors were subdued across all populations (Figure 4I; Figure S5M). However, a 1 day release of the rapamycin led to a resumption of transcriptome dynamics and recovery of activated SSC and early progenitor numbers to control levels (Figure 4J; Figures S5A, S5B, and S5N). Altogether, these data confirm that the activated SSC to early progenitor transition is regulated by mTORC1; they also reveal that changes in the activated SSC and early progenitor proportions resulted from a rapamycin-dependent block in state transitions and pointed to responsible alterations in the transcriptome (Figure 4K).

We specifically examined differential mRNA levels between spermatogonia from control and rapamycin-treated testes (Table S3) and found 4,467 genes altered by rapamycin, 336 of which were lower in all undifferentiated spermatogonia following rapamycin treatment (Figure 4L; Table S4). GO categories for these genes included “positive regulation of transcription, DNA-templated,” “transcription elongation from RNA polymerase II promoter,” “regulation of transcription from RNA polymerase II promoter,” “negative regulation of transcription from RNA polymerase II promoter,” and “mRNA processing” (Figure S6A; Table S5). In general, mTORC1 inhibition appears to have broadly suppressed the transcription machinery, resulting in reduced mRNA levels across the genome (Figure S6B). In addition, genes suppressed by rapamycin uniquely in quiescent SSCs were enriched for the GO terms “translational termination,” “mRNA splicing, via spliceosome,” “mRNA processing,” and “RNA splicing, via transesterification reactions with bulged adenosine as nucleophile” (Table S5), suggesting that mTORC1 regulates gene expression in quiescent SSCs at the post-transcriptional level. Genes involved in cell-cycle phase transitions were suppressed by rapamycin in both activated SSCs and late progenitors (Table S5), indicating mTORC1 regulates the proliferative state.

Of particular interest were genes uniquely downregulated by rapamycin in early progenitors, because mTORC1 was necessary for their formation from activated SSCs. The 27 genes specifically suppressed by rapamycin in early progenitors were significantly enriched for the

GO terms “regulation of insulin-like growth factor receptor signaling pathway,” “negative regulation of canonical Wnt signaling pathway,” “negative regulation of Wnt signaling pathway,” and “regulation of canonical Wnt signaling pathway” (Table S5). These data suggest that mTORC1 regulates the transition of activated SSCs to early progenitors via the inhibition of insulin-like growth factor receptor (IGFR) signaling and the activation of Wnt signaling, in agreement with prior results indicating that activation of the IGFR signaling pathway and inhibition of the Wnt signaling pathway are necessary for SSC renewal (Takase and Nusse, 2016; Tokue et al., 2017; Wang et al., 2015). Two genes common to these enriched GO terms in early progenitors were *Igfbp2* and *Igfbp6*, which are insulin growth factor (IGF) signaling inhibitors (Allard and Duan, 2018). We also found that *Igfbp2* mRNA was expressed by all SSC and progenitor populations, whereas *Igfbp6* mRNA was detectable only in early and late progenitors. Both mRNAs were significantly suppressed by mTORC1 inhibition in early progenitors (Figures S6C–S6H). Altogether, these data indicate that mTORC1 not only influences genome-wide transcription in all spermatogonia but also drives specific gene expression programs involved in transitions among spermatogonial subtypes (Figure 4; Tables S3, S4, and S5).

mTORC1 regulates the interconversion between activated SSCs and clones of early progenitors

Finally, to investigate whether spermatogonial clone size is relevant to the dynamics among SSCs and progenitors (Figure 4K), we confirmed the proportion of SSC and progenitor subsets in post-natal day 36 (P36) *Tex14*$^{-/-}$ testes, which lack intercellular bridges and in which spermatogonia remain isolated (Greenbaum et al., 2006). The proportion of each spermatogonial population in P36 *Tex14*$^{-/-}$ testes was largely unchanged compared with P36 *Tex14*$^{+/-}$ testes (Figures 5A–5D), indicating that early and late progenitors can exist as isolated, single spermatogonia and intercellular bridges are not required for the SSC-to-progenitor transition at P36 before steady-state spermatogenesis. These data also refute the dogmatic A_{single} model assertion that progenitors must exist as clones of two or more spermatogonia.

To test the hypothesis that mTORC1 induces activated SSCs to produce clones of early progenitors, we treated P36 *Tex14*$^{-/-}$ mice with rapamycin. Although rapamycin caused accumulation of activated SSCs and depletion of early progenitors (Figures 3G and 3H) in the wild-type testis, rapamycin-treated P36 *Tex14*$^{-/-}$ testes failed to accumulate activated SSCs and exhibited impeded early progenitor proliferation (Figures 5C and 5D). Thus, steady-state mTORC1 signaling drives activated SSCs to produce progenitor clones, which are absent from *Tex14*$^{-/-}$ testes. These data also indicate that a significant proportion of the SSC-to-progenitor transition is independent of mTORC1 and occurs within the A_{single} spermatogonial pool. We predicted that if SSC renewal at least partially depended on reversion from clones of early progenitors, SSC numbers should decline in adulthood in *Tex14*$^{-/-}$ mice. To test thishypothesis, we examined spermatogonial proportions in testes from 2- to 3-month-old adult *Tex14*$^{-/-}$ mice (Figures 5E and 5F). We found that the proportion of SSCs was significantly reduced by 1.74-fold, with a reciprocally significant 1.58-fold increase in early progenitors, despite a significant reduction in early progenitor proliferation (Figures 5E and 5F). Altogether, these results are consistent with the reversion

of unstable early progenitor spermatogonia clones to activated SSCs, as predicted by RNA velocity analysis. mTORC1 signaling appears to favor the state transition from activated SSC to early progenitor, whereas mTORC1 inhibition favors self-renewal and reacquisition of the activated SSC phenotype, as proposed by the fragmentation model (Figures 4K and 5G).

DISCUSSION

SSCs have been characterized by marker protein expression (e.g., GFRA1), expression of transgenic reporters (e.g., *Id4*-eGFP), genetic lineage tracing with Cre recombinase drivers (e.g., *Gfra1*-Cre) (Chan et al., 2014; Hara et al., 2014; Helsel et al., 2017b; Nakagawa et al., 2007, 2010; Sun et al., 2015; Yoshida et al., 2006), and epigenomic profiling (Cheng et al., 2020), and can be experimentally distinguished from progenitors by their ability to perpetually self-renew and initiate spermatogenic differentiation (Helsel et al., 2017b; Hermann et al., 2018; La et al., 2018b; Mutoji et al., 2016; Sun et al., 2015). To date, however, no single marker or label has been identified (and verified) that selectively and prospectively recognizes SSCs (Hermann et al., 2018; Mutoji et al., 2016). We previously reported comprehensive gene expression profiles that distinguish transplantation-validated SSCs and progenitors (Hermann et al., 2018), but these static observations/analyses were difficult to extrapolate to the dynamic relationships among cell states. To overcome this limitation, we employed RNA velocity analysis in the present study to empirically establish SSC-progenitor relationships and define mechanisms driving spermatogonial fate transitions in the mouse testis *in vivo*.

Our data support the presence of a dominant population of quiescent SSCs (Figures 2E–2H; Figures S4G–S4I). The low SSC Ki67-labeling index we observed in adult testes is consistent with independent data from previous studies (Grasso et al., 2012; Hara et al., 2014; Lok and de Rooij, 1983; Sharma et al., 2019). Importantly, we use the term “quiescent” to refer to the state of cells at the moment we assess them, which is not necessarily indicative of a permanently quiescent (e.g., reserve SSC) subpopulation. These results are also consistent with the SSC pool being largely quiescent in steady state but a small proportion becoming stochastically activated.

Several notable niche-derived extrinsic factors (e.g., glial cell line-derived neurotrophic factor [GDNF]) and germline intrinsic factors (e.g., GFRA1 and ID4) have been shown to direct SSC proliferation (Chan et al., 2014; Kitadate et al., 2019; Mutoji et al., 2016; Nakagawa et al., 2010; Oatley et al., 2009; Takashima et al., 2015). GDNF stimulates GFRA1/RET signaling to maintain SSC numbers via the activation of PI3K-AKT/MAPK (Oatley et al., 2007; Takashima et al., 2015) or rat sarcoma viral oncogene (RAS) (Oatley et al., 2007) signaling pathways to drive proliferation (Ishii et al., 2012; Uchida et al., 2016; Wang et al., 2017), although pharmacological levels GDNF also appear to suppress SSC proliferation *in vitro* and *in vivo* (Helsel et al., 2017a; Kanatsu-Shinohara et al., 2019; Sharma and Braun, 2018). Here, we found that activation of MAPK and AKT signaling is coincident with the transition from quiescence to cell-cycle activation among SSCs (Figure 3). Thus, we speculate that GDNF/GFRA1/RET signaling promotes the transition from quiescence to activation among SSCs. Because SSCs and progenitors both broadly express

GFRA1 and RET, it remains unclear how the SSC and progenitor responses to GDNF are tailored to either promote proliferation or retain a quiescent state.

Of significance, we identified a switch involving mTORC1 signaling, which appears to regulate the balance between SSC self-renewal and initiation of progenitor maturation toward spermatogonial differentiation (Figures 3 and 4; Figures S5 and S6). Previous studies of the first wave of spermatogenesis established that PI3K/AKT-dependent mTORC1 signaling is required for spermatogonial differentiation (Busada et al., 2015b; Serra et al., 2017). Here we show that mTORC1 activation is also permissive of spermatogonial differentiation in the adult testis. These findings are consistent with data from studies of yeast showing that inhibition of TORC1 signaling induces the G0 program of transcriptional repression (Zaragoza et al., 1998) and studies of mammals in which mTORC1 regulates (1) mRNA translation via p-RPS6 kinase (Valvezan and Manning, 2019) and (2) activity of RNA polymerase I (RNA Pol I) and RNA polymerase III (RNA Pol III) (Ma and Blenis, 2009). Our results demonstrate that mTORC1 inhibition changed the relative proportions of activated SSCs and early progenitors accompanied by genome-wide transcriptional repression and cell-type-specific gene expression changes *in vivo* (Figure 4L; Figures S6A and S6B), raising the exciting possibility that mTORC1 signaling regulates gene expression at both translational and transcriptional levels in undifferentiated spermatogonia.

Nearly all A_{paired} (A_{pr}) and $A_{aligned}$ (A_a) spermatogonia convert to A1-differentiating spermatogonia in response to the pulse of RA that occurs at the midpoint of the cycle of the seminiferous epithelium (Busada et al., 2015a; Zhou et al., 2008). Here we show that RA signaling also enhances the proliferation of early progenitors (Figures S4C and S4D), which lack expression of RARγ (Figure 1B; Figures S3A–S3C, S5C, S5F, and S5I), the canonical RAR that is both necessary and sufficient for spermatogonial differentiation (Gely-Pernot et al., 2012; Ikami et al., 2015). One possible explanation is that RA-dependent early progenitor proliferation is mediated indirectly through other RAR-expressing cell types (Raverdeau et al., 2012). Alternatively, it is possible that RARα may be expressed by spermatogonia and participate in regulating their fate (Ikami et al., 2015; Peer et al., 2018).

Limitations of the study

The complexity of spermatogonial single-cell datasets is high, and although we have attempted to judiciously define cell populations based on a robust marker gene set, our effort to reduce the complexity necessarily caused us to exclude some cell populations with hybrid gene expression profiles. The precise temporal position of these and similar intermediate cell populations along the spermatogonial continuum is unclear, highlighting the need to develop additional strict phenotypic definitions for cell states supported by functional readouts. Because the scRNA-seq methodology underlying our RNA velocity analysis is, by its nature, a destructive technique, a limitation of RNA velocity analysis is the inability to definitively follow developmental changes over time. Despite this limitation, the velocyto algorithm (and others) has been used to infer cell states and metastability (Zywitza et al., 2018; Wang et al., 2020; Xia et al., 2019; Bergen et al., 2020), including among human spermatogonia (Guo et al., 2018). More definitive confirmation of cell-state transitions at the resolution of SSC and progenitor subtypes would require future live imaging or genetic lineage tracing. In

particular, the potential for progenitor reversion to SSCs raised by our work in *Tex14*$^{-/-}$ testes lacking spermatogonial clones awaits future examination. Moreover, it is important to acknowledge the potential for differential post-transcriptional gene regulation to alter protein-level expression patterns implied by mRNA-level patterns.

Conclusions

In this study, we establish a stepwise understanding of SSC fate decisions and the molecular logic for undertaking those alternate fates. We propose that this process involves two discrete transition states between SSCs and progenitor spermatogonia in mouse testes (Figure 4K). First, subsets of SSCs bidirectionally interconvert between quiescent and activated cell-cycle states in a manner coincident with MAPK and PI3K/AKT signaling activity. We posit that niche-derived GDNF is instructive in SSC cell-cycle activation. Subsequently, mTORC1 toggles the fate of activated SSCs to early progenitor clones in a manner influenced by RA to initiate differentiation (Figure 4K). Although still not definitively resolved, because early progenitor spermatogonia exhibit transcriptome signatures that appear to favor transition to either SSCs or late progenitors, it remains possible that bidirectional interconversion between SSCs and clones of progenitors consistent with clone fragmentation contributes to SSC self-renewal in steady state (Hara et al., 2014; Nakagawa et al., 2007, 2010).

STAR★METHODS

RESOURCE AVAILABILITY

Lead contact—Further information and requests for resources and reagents should be directed to and will be fulfilled by the Lead Contact, Brian Hermann (Brian.Hermann@utsa.edu).

Materials availability—This study did not generate new unique reagents.

Data and code availability—All datasets (raw and analyzed) produced in the conduct of these studies are publically available at NIH GEO and Mendeley Data (see Key resources table). The custom GRCm38 (mouse mm10) reference dataset containing the EGFP cDNA sequence used for 10x Genomics single-cell analysis is available for download (Mendeley Data: https://doi.org/10.17632/xzk2zyymxy.1). There are no restrictions for the use of these data or resources in future studies. Previously published and publically available data were used for Figures 1 and S1 [GEO: GSE152930; (Hermann et al., 2018)] and Figure S2 [GEO: GSE109033, (La et al., 2018b)]. Raw and processed data for Figures 4 and S5 were deposited under accession numbers GEO: GSE152930 (see Key resources table). The code supporting the content of this study is available upon request.

EXPERIMENTAL MODEL AND SUBJECT DETAILS

All experiments utilizing animals were approved by the Institutional Animal Care and Use Committees of the University of Texas at San Antonio (Assurance A3592–01) and were performed in accordance with the NIH Guide for the Care and Use of Laboratory Animals. All animals were maintained under conditions of *ad libitum* water and food with constant

light-dark cycles. Mice were treated as follows: (1) a single 100 μL bolus of 7.5 mg/mL all-*trans*RA (Sigma-Aldrich) as described (Endo et al., 2015) and euthanized 24 hours later, (2) four 100 μL injections of 20 mg/mL WIN18,446 (sc-295819A; Santa Cruz Biotechnology) as described (Endo et al., 2015) at 12 hour intervals and euthanized 12 hours after the final injection, or (3) two 100 μL injections of 0.8 mg/mL rapamycin (Biotang Inc.) as described (Hobbs et al., 2010) separated by 24 hours and euthanized 24 hours, 48 hours, or 72 hours after the second injection (see Figure 4A). Male C57BL/6 wild-type and Id4-Egfp transgenic mice congenic on the C57BL/6 background (Chan et al., 2014) were used as adults (between 2 and 6 months of age) and male *Tex14*+/− and *Tex14*−/− mice (Greenbaum et al., 2006) were used at post-natal day 36 when normal spermatogonial populations are still present and also as adults (between 2 and 3 months).

METHOD DETAILS

Immunofluorescence—For whole-mount immunofluorescence, seminiferous tubules were mechanically teased apart and rinsed in PBS, fixed with 4% paraformaldehyde (PFA) for 3 h at 4°C, washed 3X in PBS, and blocked in PBS containing 0.3% Triton X-100, 10% FBS and 2% BSA. Seminiferous tubules were then incubated overnight at 4°C with primary antibodies (see list of antibodies and dilutions in Key resources table) diluted in PBS supplemented with 1% BSA (PBS/BSA). Note that EGFP signal was from epifluorescence, not antibody labeling. After washing three times in PBS for 15 min each, samples were incubated in PBS/BSA containing secondary antibodies (see list of antibodies and dilutions in Key resources table) for 1 hour at RT. After washing three times in PBS/BSA for 15 min each, tubules were mounted in 50% Glycerol. Positive immunoreactivity was validated by omission of primary antibody. Fluorescently signal in stained tubules were detected at 63X magnification using an AxioImager M1 (Zeiss) and an AxioCam MRm (Zeiss) or a Zeiss LSM510 confocal microscope through the UTSA Biophotonics Core.

Analysis of the percentage of quiescent SSCs and activated SSCs in each stage—Seminiferous tubule stage in whole-mount was distinguished by adapting a peanut agglutinin (PNA) staining method (Nakata et al., 2015). Use of PNA was necessary for staging, rather than use of other antibodies, because of multiple antibodies were already needed to distinguish quiescent SSCs (PLZF+/SOX3−/Ki67−) from activated SSCs (PLZF+/SOX3−/Ki67+). We first validated that PNA labeling was sufficient for defining stage groups by co-labeling for KIT (Figure S3F), the spermatid morphologies we observed in whole mount matched the results from Nakata et al. (2015) in tissue section and separate whole-mount staining for KIT (Sharma and Braun, 2018). We were able to reliably discern three groups of stages corresponding to early (Stages I-V), mid (Stages VI-IX) and late (Stages X-XII) phases of the seminiferous epithelial cycle. To identify quiescent and activated SSC numbers by stage, we co-stained for PLZF/SOX3/Ki67/PNA and imaged the same segment of each seminiferous tubule at multiple focal planes corresponding to PNA-labeled spermatids and PLZF/SOX3/Ki67-labeled SSCs. From multiple animals, a total of 132, 128, and 134 quiescent SSCs (PLZF+/SOX3−/Ki67−) were counted in stages I-V, VI-IX, and X-X-II, respectably, and the total 27, 38, and 71 of activated SSCs (PLZF+/SOX3−/Ki67+) were counted in stages I-V, VI-IX, and X-X-II, respectably. The proportion of SSCs

that were quiescent (PLZF+/SOX3−/Ki67−) versus activated (PLZF+/SOX3−/Ki67+) was calculated in each stage and compared by ANOVA.

Generation of adult mouse seminiferous tubule cell suspensions—Single-cell suspensions from adult mouse testes were generated as previously described (Hermann et al., 2018), with minor modifications. Briefly, testicular parenchyma from an adult mice were digested with 1mg/ml Collagenase Type IV (Sigma) for 15 minutes at 37°C, washed with PBS to remove interstitial cells, digested with 0.25% trypsin/EDTA for 3 minutes at 37°C, removed 0.25% trypsin/EDTA, stopped by addition of Hank's Buffered Salt Solution (HBSS) containing 1% FBS, and pipetted until the cells were dissociated.

Flow cytometry analysis—Dissociated cells were fixed with 4% PFA for 10 min at RT. For experiments with *Id4-Egfp* transgenic mice (Chan et al., 2014), fixed cells were incubated in PBS supplemented with 1% FBS (PBS/FBS; 0.5 mL/testis) and Biotin conjugated rat anti-CD9 antibodies (1 μg/mL, clone MZ3, BioLegend) for 20 min on ice, washed with 1%PBS/FBS, and incubated in PBS/FBS supplemented with APC streptavidin (0.08 μg/mL, BioLegend) for 20 min on ice. After washing in PBS/FBS, cells were permeabilized by incubation in PBS containing 0.3% Triton X-100 for 10 min RT and then washed in PBS. For experiments with adult C57BL/6 mouse testis cells and P36 *Tex14*+/− and *Tex14*−/− (Greenbaum et al., 2006) mouse testis cells, fixed cells were permeabilized by incubation with methanol for 30 min on ice and washed in PBS. Permeabilized adult testis cells (*Id4-Egfp*, C57BL/6, *Tex14*+/−, or *Tex14*−/−) were subsequently incubated for 30 min at RT in PBS/FBS containing primary antibodies (see list of antibodies and dilutions in Key resources table). After washing twice in PBS/FBS, cells were incubated in PBS/BSA containing secondary antibodies and conjugated antibodies (see list of antibodies and dilutions in Key resources table) for 30 min at RT. After washing in PBS/FBS, fluorescent signals were detected with an LSRII cytometer (BD Biosciences) in the UTSA Cell Analysis Core and data were analyzed using FlowJo v10 software (BD Biosciences).

ID4-EGFP-bright spermatogonia isolation by FACS—Single-cell suspensions from adult *Id4-eGFP* transgenic mouse testes were generated as described above for flow cytometry analysis and subsequently used for FACS as described (Hermann et al., 2018). Testes from at least three mice were used for each preparation. Briefly, dissociated seminiferous tubule cells were suspended in ice-cold Dulbecco's phosphate-buffered saline (DPBS) containing 10% FBS (DPBS+S) and seminiferous tubule cells were pre-enriched for spermatogonia by density centrifugation in DPBS+S over a 30% Percoll cushion (Sigma) for 8 minutes at 600xg without braking. Pelleted cells were labeled with anti-CD9 antibodies (Key resources table) subjected to FACS using a FACS Aria II (BD) in the UTSA Cell Analysis Core. Spermatogonia isolated based on gating CD9-bright and ID4-EGFP double-positive cells and subgating into the brightest 33% EGFP epiflourescent cells. Positive antibody labeling was determined by comparison to staining with isotype control antibodies (see Key resources table). Positive ID4-EGFP epifluorescence was determined by comparison to testis cells from C57BL/6 males. Dead cells were discriminated with propidium iodide (Biolegend). All antibodies and their dilution for staining is noted in the Key resources table.

10x Genomics single-cell RNA-seq—Through the UTSA Genomics Core, suspensions of ~6,400 ID4-EGFP^{bright} mouse spermatogonia were loaded into Chromium micro-fluidic chips with 3′ v3 chemistry and used to generate single-cell gelbead emulsions (GEMs) for ~4,000 single cells using the Chromium controller (10x Genomics) per manufacturer recommendations (Zheng et al., 2017). Reverse transcription was performed in a T100 Thermal cycler (Bio-Rad) and all subsequent steps to generate single-cell libraries were performed according to manufacturer recommendations (User Guide CG000204 Rev D). Libraries were sequenced on an Illumina NovaSeq instrument (NovoGene, Inc.) using PE150 chemistry. Trimmed FASTQ files [Read 1 - (28bp Cell barcode & UMI), 10bp i7 index, and Read2 - 90bp) were generated using CellRanger mkfastq. Primary data analysis (alignment, filtering, and UMI counting) to determine transcript counts per cell (producing a gene-barcode matrix), quality control, clustering and statistical analysis were performed using CellRanger v3.1.0 (10x Genomics) using default settings and a customized GRCm38 (mouse mm10) reference dataset containing the EGFP cDNA sequence (see Key resources table). Quality control metrics from these new single-cell data are found in Table S6.

QUANTIFICATION AND STATISTICAL ANALYSIS

Raw read count matrices obtained from each dataset using CellRanger 3.1.0 (10x Genomics) were used to generate a log-normalized [log10(TPM+1)] expression matriz using edgeR (Robinson et al., 2010) and was used for cell clustering and t-distributed stochastic neighbor embedding (tSNE) projections. Cell clustering using a K-Nearest-Neighbor-Pooling Matching (KNNPM) method and projection/visualization (tSNE plots) RNA velocity was performed with velocyto.R (La Manno et al., 2018; Svensson and Pachter, 2018) following the Mouse BM/dropEst tutorial (http://pklab.med.harvard.edu/velocyto/notebooks/R/SCG71.nb.html) with default parameters after filtering cells with fewer than 1800 genes, and genes with fewer than 10 reads and detected in only five or fewer cells. Differential gene expression analysis was performed using TCC (Deseq2) (Sun et al., 2013) using a FDR q-value cutoff (< 0.01). Gene ontology analysis was performed using Enrichr (https://maayanlab.cloud/Enrichr/) (Chen et al., 2013; Kuleshov et al., 2016). Bioinformatic cell cycle analysis was performed as previously described (http://jdblischak.github.io/singleCellSeq/analysis) (Whitfield et al., 2002). Quantitative flow cytometry and cell counts from whole-mount stained seminiferous tubule are presented as mean ± s.e.m and significant differences between groups was determined by two-tailed Student’s t test or ANOVA (Microsoft Excel), as specified in the figure legends. The number of replicate animals per group is specified in figure legends (n = number of mice).

Supplementary Material

Refer to Web version on PubMed Central for supplementary material.

ACKNOWLEDGMENTS

Dr. Martin Matzuk and Julio Agno (Baylor College of Medicine) provided the *Tex14*$^{-/-}$ mice. This work received computational support from UTSA’s HPC cluster SHAMU, operated by the Research Computing Support Group, Office of Information Technology. Data were generated in the UTSA Genomics Core and Cell Analysis Core, which are supported by NIH grant G12 MD007591 and NSF grants DBI-1337513 and DBI-2018408. The authors would like to thank Dr. Sandra Cardona (UTSA Cell Analysis Core) and Sean Vargas (UTSA Genomics Core) for

technical assistance. This study was supported by grant R01 HD090007 (to B.P.H.) and P50 HD98593 (to J.R.M.), both from the Eunice Kennedy Shriver National Institute of Child Health and Human Development (NICHD). The graphical abstract was produced by Victoria Foor, MFA, CMI.

REFERENCES

Allard JB, and Duan C (2018). IGF-Binding Proteins: Why Do They Exist and Why Are There So Many? Front. Endocrinol. (Lausanne) 9, 117. [PubMed: 29686648]

Bergen V, Lange M, Peidli S, Wolf FA, and Theis FJ (2020). Generalizing RNA velocity to transient cell states through dynamical modeling. Nat. Biotechnol 38, 1408–1414. 10.1038/s41587-020-0591-3. [PubMed: 32747759]

Busada JT, Chappell VA, Niedenberger BA, Kaye EP, Keiper BD, Hogarth CA, and Geyer CB (2015a). Retinoic acid regulates Kit translation during spermatogonial differentiation in the mouse. Dev. Biol 397, 140–149. [PubMed: 25446031]

Busada JT, Niedenberger BA, Velte EK, Keiper BD, and Geyer CB (2015b). Mammalian target of rapamycin complex 1 (mTORC1) Is required for mouse spermatogonial differentiation *in vivo*. Dev. Biol 407, 90–102. [PubMed: 26254600]

Chan F, Oatley MJ, Kaucher AV, Yang QE, Bieberich CJ, Shashikant CS, and Oatley JM (2014). Functional and molecular features of the Id4+ germline stem cell population in mouse testes. Genes Dev. 28, 1351–1362. [PubMed: 24939937]

Chen EY, Tan CM, Kou Y, Duan Q, Wang Z, Meirelles GV, Clark NR, and Ma'ayan A (2013). Enrichr: interactive and collaborative HTML5 gene list enrichment analysis tool. BMC Bioinformatics 14, 128. [PubMed: 23586463]

Cheng K, Chen IC, Cheng CE, Mutoji K, Hale BJ, Hermann BP, Geyer CB, Oatley JM, and McCarrey JR (2020). Unique Epigenetic Programming Distinguishes Regenerative Spermatogonial Stem Cells in the Developing Mouse Testis. iScience 23, 101596. [PubMed: 33083754]

de Rooij DG (1969). Further evidence for the proposed way of spermatogonial stem cell renewal in the rat and the mouse. Z. Zellforsch. Mikrosk. Anat 99, 134–138. [PubMed: 5810775]

de Rooij DG, and Russell LD (2000). All you wanted to know about spermatogonia but were afraid to ask. J. Androl 21, 776–798. [PubMed: 11105904]

Endo T, Romer KA, Anderson EL, Baltus AE, de Rooij DG, and Page DC (2015). Periodic retinoic acid-STRA8 signaling intersects with periodic germ-cell competencies to regulate spermatogenesis. Proc. Natl. Acad. Sci. USA 112, E2347–E2356. [PubMed: 25902548]

Endo T, Freinkman E, de Rooij DG, and Page DC (2017). Periodic production of retinoic acid by meiotic and somatic cells coordinates four transitions in mouse spermatogenesis. Proc. Natl. Acad. Sci. USA 114, E10132–E10141. [PubMed: 29109271]

Feng LX, Ravindranath N, and Dym M (2000). Stem cell factor/c-kit up-regulates cyclin D3 and promotes cell cycle progression via the phosphoinosi-tide 3-kinase/p70 S6 kinase pathway in spermatogonia. J. Biol. Chem 275, 25572–25576. [PubMed: 10849422]

Gely-Pernot A, Raverdeau M, Célébi C, Dennefeld C, Feret B, Klopfenstein M, Yoshida S, Ghyselinck NB, and Mark M (2012). Spermatogonia differentiation requires retinoic acid receptor γ. Endocrinology 153, 438–449. [PubMed: 22045663]

Grasso M, Fuso A, Dovere L, de Rooij DG, Stefanini M, Boitani C, and Vicini E (2012). Distribution of GFRA1-expressing spermatogonia in adult mouse testis. Reproduction 143, 325–332. [PubMed: 22143971]

Green CD, Ma Q, Manske GL, Shami AN, Zheng X, Marini S, Moritz L, Sultan C, Gurczynski SJ, Moore BB, et al. (2018). A Comprehensive Roadmap of Murine Spermatogenesis Defined by Single-Cell RNA-Seq. Dev. Cell 46, 651–667.e10. [PubMed: 30146481]

Greenbaum MP, Yan W, Wu MH, Lin YN, Agno JE, Sharma M, Braun RE, Rajkovic A, and Matzuk MM (2006). TEX14 is essential for intercellular bridges and fertility in male mice. Proc. Natl. Acad. Sci. USA 103, 4982–4987. [PubMed: 16549803]

Guo J, Grow EJ, Mlcochova H, Maher GJ, Lindskog C, Nie X, Guo Y, Takei Y, Yun J, Cai L, et al. (2018). The adult human testis transcriptional cell atlas. Cell Res. 28, 1141–1157. [PubMed: 30315278]

Hara K, Nakagawa T, Enomoto H, Suzuki M, Yamamoto M, Simons BD, and Yoshida S (2014). Mouse spermatogenic stem cells continually interconvert between equipotent singly isolated and syncytial states. Cell Stem Cell 14, 658–672. [PubMed: 24792118]

Helsel AR, Oatley MJ, and Oatley JM (2017a). Glycolysis-Optimized Conditions Enhance Maintenance of Regenerative Integrity in Mouse Spermatogonial Stem Cells during Long-Term Culture. Stem Cell Reports 8, 1430–1441. [PubMed: 28392219]

Helsel AR, Yang QE, Oatley MJ, Lord T, Sablitzky F, and Oatley JM (2017b). ID4 levels dictate the stem cell state in mouse spermatogonia. Development 144, 624–634. [PubMed: 28087628]

Hermann BP, Cheng K, Singh A, Roa-De La Cruz L, Mutoji KN, Chen IC, Gildersleeve H, Lehle JD, Mayo M, Westernströer B, et al. (2018). The Mammalian Spermatogenesis Single-Cell Transcriptome, from Spermatogonial Stem Cells to Spermatids. Cell Rep. 25, 1650–1667. [PubMed: 30404016]

Hobbs RM, Seandel M, Falciatori I, Rafii S, and Pandolfi PP (2010). Plzf regulates germline progenitor self-renewal by opposing mTORC1. Cell 142, 468–479. [PubMed: 20691905]

Huckins C (1971). The spermatogonial stem cell population in adult rats. I. Their morphology, proliferation and maturation. Anat. Rec 169, 533–557. [PubMed: 5550532]

Ikami K, Tokue M, Sugimoto R, Noda C, Kobayashi S, Hara K, and Yoshida S (2015). Hierarchical differentiation competence in response to retinoic acid ensures stem cell maintenance during mouse spermatogenesis. Development 142, 1582–1592. [PubMed: 25858458]

Ishii K, Kanatsu-Shinohara M, Toyokuni S, and Shinohara T (2012). FGF2 mediates mouse spermatogonial stem cell self-renewal via upregulation of Etv5 and Bcl6b through MAP2K1 activation. Development 139, 1734–1743. [PubMed: 22491947]

Kanatsu-Shinohara M, Yamamoto T, Toh H, Kazuki Y, Kazuki K, Imoto J, Ikeo K, Oshima M, Shirahige K, Iwama A, et al. (2019). Aging of spermatogonial stem cells by Jnk-mediated glycolysis activation. Proc. Natl. Acad. Sci. USA 116, 16404–16409. [PubMed: 31358627]

Kitadate Y, Jörg DJ, Tokue M, Maruyama A, Ichikawa R, Tsuchiya S, Segi-Nishida E, Nakagawa T, Uchida A, Kimura-Yoshida C, et al. (2019). Competition for Mitogens Regulates Spermatogenic Stem Cell Homeostasis in an Open Niche. Cell Stem Cell 24, 79–92.e6. [PubMed: 30581080]

Kuleshov MV, Jones MR, Rouillard AD, Fernandez NF, Duan Q, Wang Z, Koplev S, Jenkins SL, Jagodnik KM, Lachmann A, et al. (2016). Enrichr: a comprehensive gene set enrichment analysis web server 2016 update. Nucleic Acids Res. 44 (W1), W90–W97. [PubMed: 27141961]

La HM, Chan AL, Legrand JMD, Rossello FJ, Gangemi CG, Papa A, Cheng Q, Morand EF, and Hobbs RM (2018a). GILZ-dependent modulation of mTORC1 regulates spermatogonial maintenance. Development 145, dev165324. [PubMed: 30126904]

La HM, Mäkelä JA, Chan AL, Rossello FJ, Nefzger CM, Legrand JMD, De Seram M, Polo JM, and Hobbs RM (2018b). Identification of dynamic undifferentiated cell states within the male germline. Nat. Commun 9, 2819. [PubMed: 30026551]

La Manno G, Soldatov R, Zeisel A, Braun E, Hochgerner H, Petukhov V, Lidschreiber K, Kastriti ME, Lönnerberg P, Furlan A, et al. (2018). RNA velocity of single cells. Nature 560, 494–498. [PubMed: 30089906]

Lafzi A, Moutinho C, Picelli S, and Heyn H (2018). Tutorial: guidelines for the experimental design of single-cell RNA sequencing studies. Nat. Protoc 13, 2742–2757. [PubMed: 30446749]

Lauridsen FKB, Jensen TL, Rapin N, Aslan D, Wilhelmson AS, Pundhir S, Rehn M, Paul F, Giladi A, Hasemann MS, et al. (2018). Differences in Cell Cycle Status Underlie Transcriptional Heterogeneity in the HSC Compartment. Cell Rep. 24, 766–780. [PubMed: 30021172]

Li L, Dong J, Yan L, Yong J, Liu X, Hu Y, Fan X, Wu X, Guo H, Wang X, et al. (2017). Single-Cell RNA-Seq Analysis Maps Development of Human Germline Cells and Gonadal Niche Interactions. Cell Stem Cell 20, 891–892. [PubMed: 28575695]

Lok D, and de Rooij DG (1983). Spermatogonial multiplication in the Chinese hamster. III. Labelling indices of undifferentiated spermatogonia throughout the cycle of the seminiferous epithelium. Cell Tissue Kinet. 16, 31–40. [PubMed: 6681735]

Lord T, and Oatley JM (2017). A revised A_{single} model to explain stem cell dynamics in the mouse male germline. Reproduction 154, R55–R64. [PubMed: 28624768]

Lukassen S, Bosch E, Ekici AB, and Winterpacht A (2018). Characterization of germ cell differentiation in the male mouse through single-cell RNA sequencing. Sci. Rep 8, 6521. [PubMed: 29695820]

Ma XM, and Blenis J (2009). Molecular mechanisms of mTOR-mediated translational control. Nat. Rev. Mol. Cell Biol 10, 307–318. [PubMed: 19339977]

Mutoji K, Singh A, Nguyen T, Gildersleeve H, Kaucher AV, Oatley MJ, Oatley JM, Velte EK, Geyer CB, Cheng K, et al. (2016). TSPAN8 Expression Distinguishes Spermatogonial Stem Cells in the Prepubertal Mouse Testis. Biol. Reprod 95, 117. [PubMed: 27733379]

Nakagawa T, Nabeshima Y, and Yoshida S (2007). Functional identification of the actual and potential stem cell compartments in mouse spermatogenesis. Dev. Cell 12, 195–206. [PubMed: 17276338]

Nakagawa T, Sharma M, Nabeshima Y, Braun RE, and Yoshida S (2010). Functional hierarchy and reversibility within the murine spermatogenic stem cell compartment. Science 328, 62–67. [PubMed: 20299552]

Nakata H, Wakayama T, Takai Y, and Iseki S (2015). Quantitative analysis of the cellular composition in seminiferous tubules in normal and genetically modified infertile mice. J. Histochem. Cytochem 63, 99–113. [PubMed: 25411188]

Oakberg EF (1971). Spermatogonial stem-cell renewal in the mouse. Anat. Rec 169, 515–531. [PubMed: 5550531]

Oatley JM, Avarbock MR, Telaranta AI, Fearon DT, and Brinster RL (2006). Identifying genes important for spermatogonial stem cell self-renewal and survival. Proc. Natl. Acad. Sci. USA 103, 9524–9529. [PubMed: 16740658]

Oatley JM, Avarbock MR, and Brinster RL (2007). Glial cell line-derived neurotrophic factor regulation of genes essential for self-renewal of mouse spermatogonial stem cells is dependent on Src family kinase signaling. J. Biol. Chem 282, 25842–25851. [PubMed: 17597063]

Oatley JM, Oatley MJ, Avarbock MR, Tobias JW, and Brinster RL (2009). Colony stimulating factor 1 is an extrinsic stimulator of mouse spermatogonial stem cell self-renewal. Development 136, 1191–1199. [PubMed: 19270176]

Peer NR, Law SM, Murdoch B, Goulding EH, Eddy EM, and Kim K (2018). Germ Cell-Specific Retinoic Acid Receptor α Functions in Germ Cell Organization, Meiotic Integrity, and Spermatogonia. Endocrinology 159, 3403–3420. [PubMed: 30099545]

Raverdeau M, Gely-Pernot A, Féret B, Dennefeld C, Benoit G, Davidson I, Chambon P, Mark M, and Ghyselinck NB (2012). Retinoic acid induces Sertoli cell paracrine signals for spermatogonia differentiation but cell autonomously drives spermatocyte meiosis. Proc. Natl. Acad. Sci. USA 109, 16582–16587. [PubMed: 23012458]

Robinson MD, McCarthy DJ, and Smyth GK (2010). edgeR: a Bioconductor package for differential expression analysis of digital gene expression data. Bioinformatics 26, 139–140. [PubMed: 19910308]

Serra ND, Velte EK, Niedenberger BA, Kirsanov O, and Geyer CB (2017). Cell-autonomous requirement for mammalian target of rapamycin (Mtor) in spermatogonial proliferation and differentiation in the mouse†. Biol. Reprod 96, 816–828. [PubMed: 28379293]

Sharma M, and Braun RE (2018). Cyclical expression of GDNF is required for spermatogonial stem cell homeostasis. Development 145, dev151555. [PubMed: 29440301]

Sharma M, Srivastava A, Fairfield HE, Bergstrom D, Flynn WF, and Braun RE (2019). Identification of EOMES-expressing spermatogonial stem cells and their regulation by PLZF. eLife 8, e43352. [PubMed: 31149899]

Song HW, Bettegowda A, Lake BB, Zhao AH, Skarbrevik D, Babajanian E, Sukhwani M, Shum EY, Phan MH, Plank TM, et al. (2016). The Homeobox Transcription Factor RHOX10 Drives Mouse Spermatogonial Stem Cell Establishment. Cell Rep. 17, 149–164. [PubMed: 27681428]

Sun J, Nishiyama T, Shimizu K, and Kadota K (2013). TCC: an R package for comparing tag count data with robust normalization strategies. BMC Bioinformatics 14, 219. [PubMed: 23837715]

Sun F, Xu Q, Zhao D, and Degui Chen C (2015). Id4 Marks Spermatogonial Stem Cells in the Mouse Testis. Sci. Rep 5, 17594. [PubMed: 26621350]

Suzuki S, Diaz VD, and Hermann BP (2019). What has single-cell RNA-seq taught us about mammalian spermatogenesis? Biol. Reprod 101, 617–634. [PubMed: 31077285]

Svensson V, and Pachter L (2018). RNA Velocity: Molecular Kinetics from Single-Cell RNA-Seq. Mol. Cell 72, 7–9. [PubMed: 30290149]

Takase HM, and Nusse R (2016). Paracrine Wnt/β-catenin signaling mediates proliferation of undifferentiated spermatogonia in the adult mouse testis. Proc. Natl. Acad. Sci. USA 113, E1489–E1497. [PubMed: 26929341]

Takashima S, Kanatsu-Shinohara M, Tanaka T, Morimoto H, Inoue K, Ogonuki N, Jijiwa M, Takahashi M, Ogura A, and Shinohara T (2015). Functional differences between GDNF-dependent and FGF2-dependent mouse spermatogonial stem cell self-renewal. Stem Cell Reports 4, 489–502. [PubMed: 25684228]

Tokue M, Ikami K, Mizuno S, Takagi C, Miyagi A, Takada R, Noda C, Kitadate Y, Hara K, Mizuguchi H, et al. (2017). SHISA6 Confers Resistance to Differentiation-Promoting Wnt/β-Catenin Signaling in Mouse Spermatogenic Stem Cells. Stem Cell Reports 8, 561–575. [PubMed: 28196692]

Uchida A, Kishi K, Aiyama Y, Miura K, Takase HM, Suzuki H, Kanai-Azuma M, Iwamori T, Kurohmaru M, Tsunekawa N, and Kanai Y (2016). *In vivo* dynamics of GFRα1-positive spermatogonia stimulated by GDNF signals using a bead transplantation assay. Biochem. Biophys. Res. Commun 476, 546–552. [PubMed: 27255992]

Valvezan AJ, and Manning BD (2019). Molecular logic of mTORC1 signalling as a metabolic rheostat. Nat. Metab 1, 321–333. [PubMed: 32694720]

Wang S, Wang X, Wu Y, and Han C (2015). IGF-1R signaling is essential for the proliferation of cultured mouse spermatogonial stem cells by promoting the G2/M progression of the cell cycle. Stem Cells Dev. 24, 471–483. [PubMed: 25356638]

Wang M, Guo Y, Wang M, Zhou T, Xue Y, Du G, Wei X, Wang J, Qi L, Zhang H, et al. (2017). The Glial Cell-Derived Neurotrophic Factor (GDNF)-responsive Phosphoprotein Landscape Identifies Raptor Phosphorylation Required for Spermatogonial Progenitor Cell Proliferation. Mol. Cell. Proteomics 16, 982–997. [PubMed: 28408662]

Wang S, Drummond ML, Guerrero-Juarez CF, Tarapore E, MacLean AL, Stabell AR, Wu SC, Gutierrez G, That BT, Benavente CA, et al. (2020). Single cell transcriptomics of human epidermis identifies basal stem cell transition states. Nat. Commun 11, 10. 10.1038/s41467-020-18075-7. [PubMed: 31900408]

Whitfield ML, Sherlock G, Saldanha AJ, Murray JI, Ball CA, Alexander KE, Matese JC, Perou CM, Hurt MM, Brown PO, and Botstein D (2002). Identification of genes periodically expressed in the human cell cycle and their expression in tumors. Mol. Biol. Cell 13, 1977–2000. [PubMed: 12058064]

Wickham H (2016). ggplot2: Elegant Graphics for Data Analysis (Springer-Verlag New York), ISBN 978-3-319-24277-4. https://ggplot2.tidyverse.org.

Xia C, Fan J, Emanuel G, Hao J, and Zhuang X (2019). Spatial transcriptome profiling by MERFISH reveals subcellular RNA compartmentalization and cell cycle-dependent gene expression. Proc. Natl. Acad. Sci. USA 116, 19490–19499. 10.1073/pnas.1912459116. [PubMed: 31501331]

Yoshida S, Sukeno M, Nakagawa T, Ohbo K, Nagamatsu G, Suda T, and Nabeshima Y (2006). The first round of mouse spermatogenesis is a distinctive program that lacks the self-renewing spermatogonia stage. Development 133, 1495–1505. [PubMed: 16540512]

Zaragoza D, Ghavidel A, Heitman J, and Schultz MC (1998). Rapamycin induces the G0 program of transcriptional repression in yeast by interfering with the TOR signaling pathway. Mol. Cell. Biol 18, 4463–4470. [PubMed: 9671456]

Zheng GX, Terry JM, Belgrader P, Ryvkin P, Bent ZW, Wilson R, Ziraldo SB, Wheeler TD, McDermott GP, Zhu J, et al. (2017). Massively parallel digital transcriptional profiling of single cells. Nat. Commun 8, 14049. 10.1038/ncomms14049. [PubMed: 28091601]

Zhou Q, Li Y, Nie R, Friel P, Mitchell D, Evanoff RM, Pouchnik D, Banasik B, McCarrey JR, Small C, and Griswold MD (2008). Expression of stimulated by retinoic acid gene 8 (Stra8) and maturation of murine gonocytes and spermatogonia induced by retinoic acid *in vitro*. Biol. Reprod 78, 537–545. [PubMed: 18032419]

Zywitza V, Misios A, Bunatyan L, Willnow TE, and Rajewsky N (2018). Single-Cell Transcriptomics Characterizes Cell Types in the Subventricular Zone and Uncovers Molecular Defects Impairing Adult Neurogenesis. Cell Rep 25, 2457–2469. 10.1016/j.celrep.2018.11.003. [PubMed: 30485812]

Highlights

- RNA velocity identifies subsets of adult mouse SSCs and progenitor spermatogonia
- Quiescent and cell-cycle-activated SSCs interconvert based on PI3K/MAPK signaling
- Steady-state mTORC1 signaling drives activated SSCs to produce progenitor clones
- mTORC1 inhibition blocks the SSC-to-progenitor transition

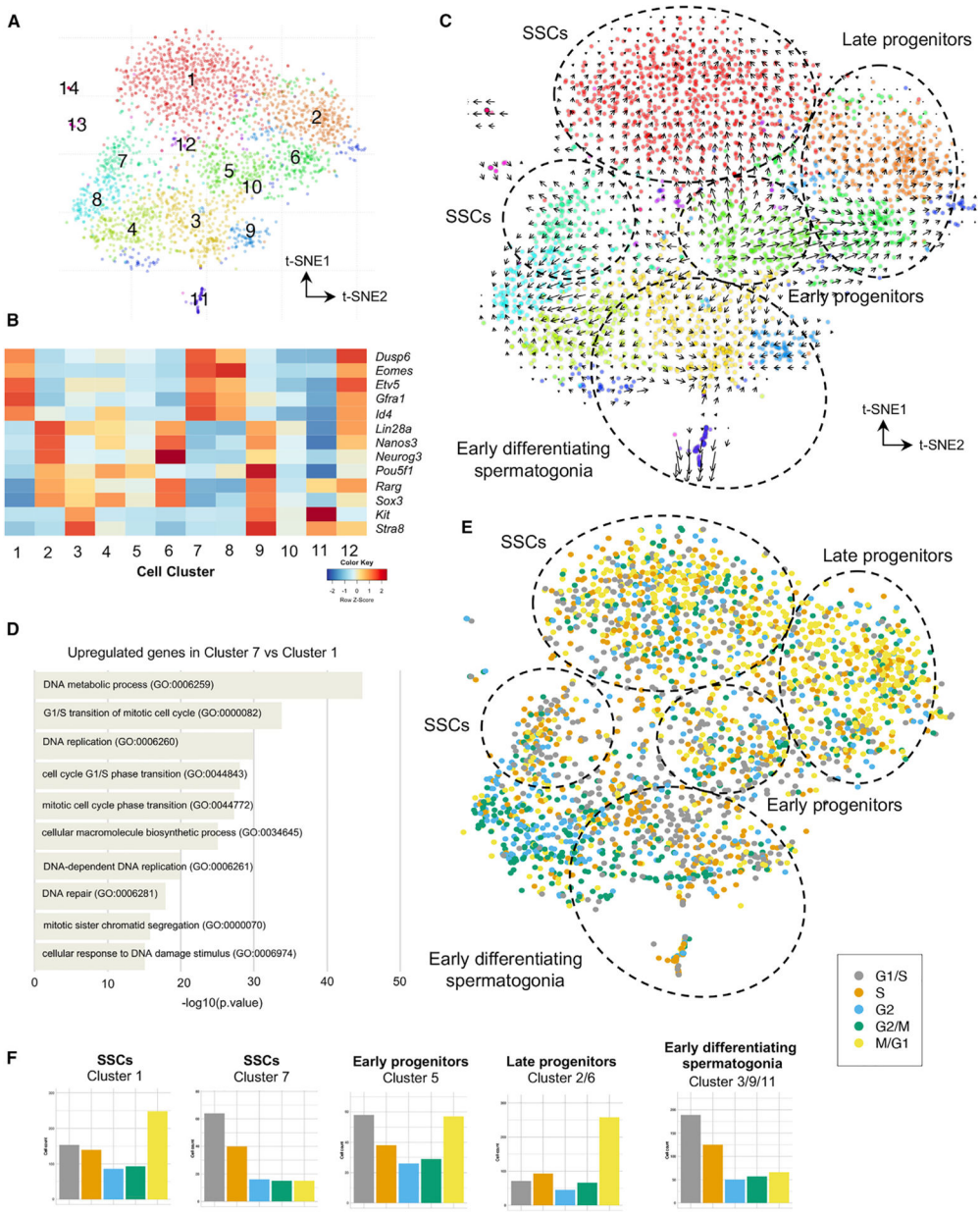

Figure 1. RNA velocity analysis predicts heterogeneous cell-cycle states and fate among adult SSCs and progenitors

(A) RNA velocity clustering of individual adult ID4-EGFP^{Bright} spermatogonia projected onto a t-distributed stochastic neighbor embedding (tSNE) plot. Clusters are color coded and numbered.

(B) Heatmap of marker gene expression collapsed from each cluster, with mRNA levels according to the Z score scale.

(C) RNA velocity vector fields indicate the observed (dots) and extrapolated future (arrows) states of adult ID4-EGFP^{Bright} spermatogonia. Cell types are noted with dashed ovals and labels.

(D) GO analysis of differentially expressed genes (DEGs) (Table S1) in SSCs from cluster 7 versus cluster 1.

(E) Cell-cycle phase analysis of adult ID4-EGFP^{Bright} spermatogonia.

(F) Proportion of cells in each cell-cycle phase grouping for clusters 1, 7, 5, 2/6, and 3/9/11.

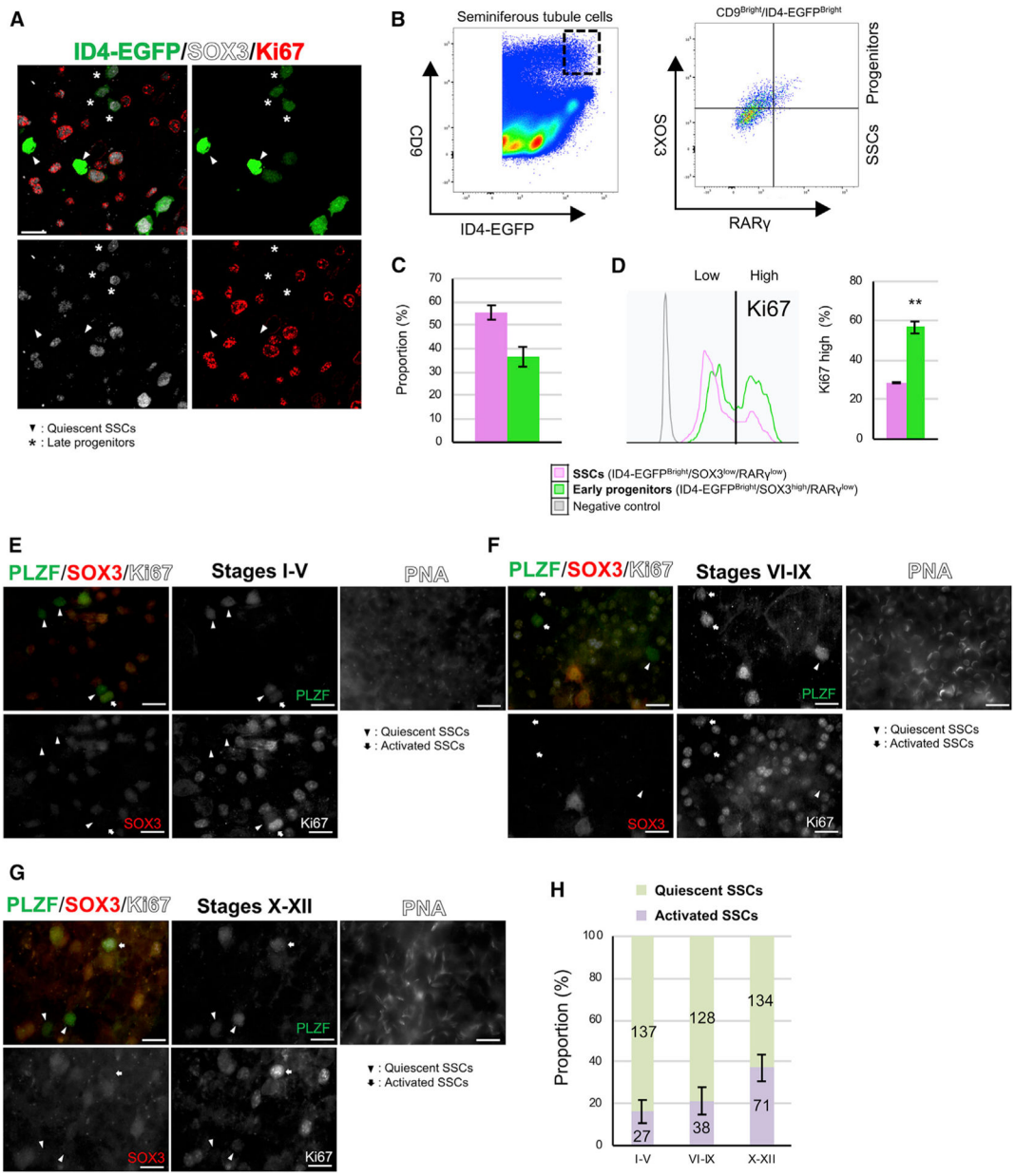

Figure 2. Cell-cycle-activated and quiescent SSCs are present throughout the cycle of the seminiferous epithelium *in vivo*

(A) Whole-mount immunofluorescence (WM-IIF) of SOX3 (white) and Ki67 (red), together with ID4-EGFP epifluorescence (green) in seminiferous tubules from adult *Id4-Egfp* mice. Scale bar, 20 μm. Arrowhead, quiescent SSCs (ID4-EGFP^{Bright}/SOX3−/Ki67−); asterisk, late progenitors (ID4-EGFP^{Dim}/SOX3+/Ki67−).

(B) Flow cytometry analysis of adult *Id4-Egfp* mouse seminiferous tubule cells sequentially gated for SSC-enriched CD9^{Bright}/ID4-EGFP^{Bright} spermatogonia (left) and SOX3 and RARγ staining (right). Figure S3H shows negative controls.

(C) Quadrant statistics from the right panel of (B). Data are mean ± SEM (n = 3 adult *Id4-Egfp* mice).

(D) Quantification of Ki67 staining intensity in cells from (B) grouped by ID4-EGFP^{Bright}/SOX3^{low}/RARγ^{low} (SSCs) or ID4-EGFP^{Bright}/SOX3^{high}/RARγ^{low} (early progenitors). Data are mean ± SEM. Two-tailed Student's t test (**$p < 0.01$).

(E–G) WM-IIF of PLZF (green), SOX3 (red), Ki67 (white), and peanut agglutinin (PNA) in adult C57BL/6 mice (n = 4). Scale bar, 20 μm. Arrowhead, quiescent SSCs (PLZF+/SOX3−/Ki67−); arrow, activated SSCs (PLZF+/SOX3−/Ki67+).

(H) Proportion of quiescent SSCs and activated SSCs in each stage from (E) and (F). Data are mean ± SEM. The proportion of Ki67+ SSCs was not significantly different according to ANOVA ($p = 0.093$).

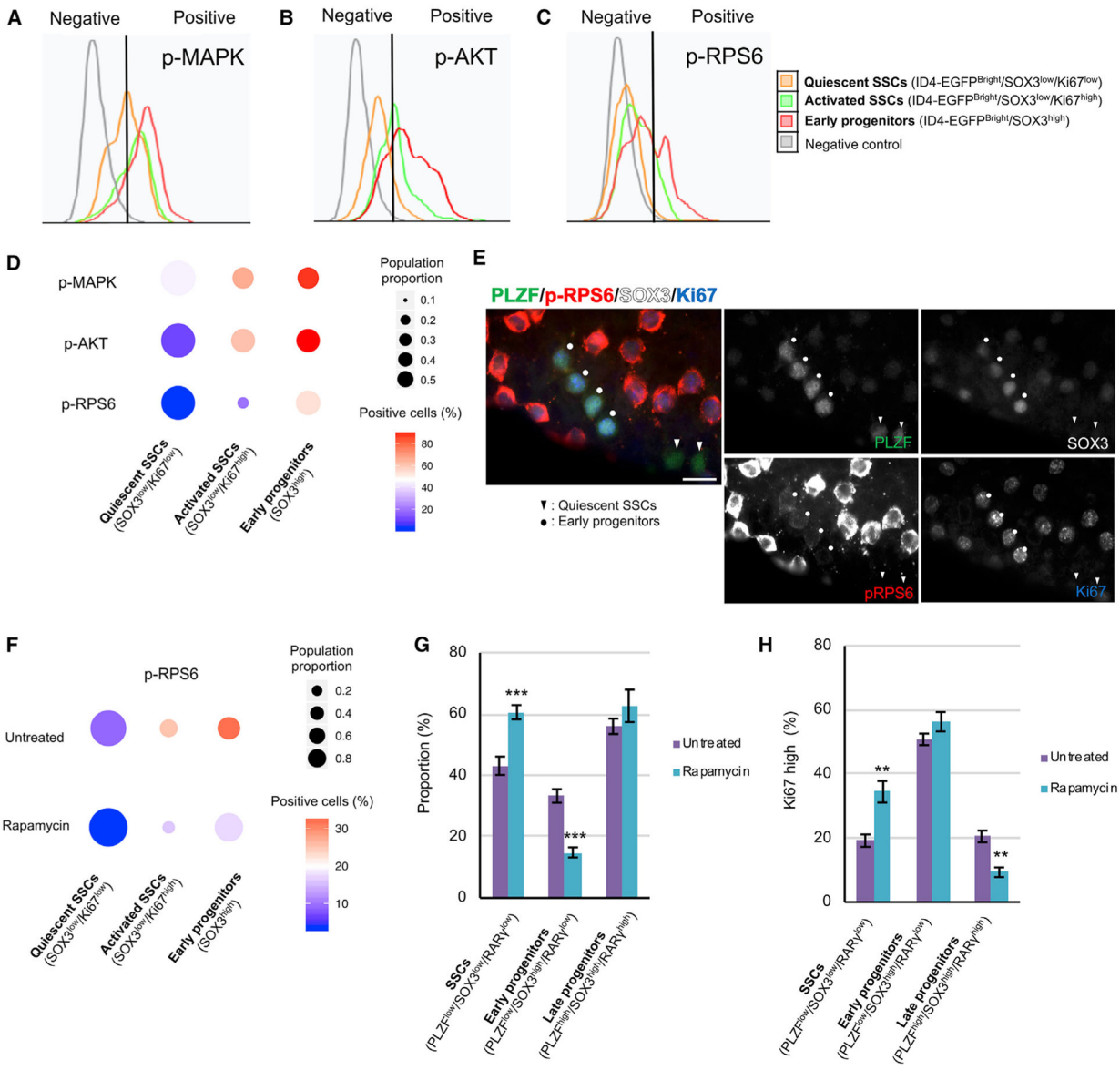

Figure 3. Signaling pathways that regulate transitions in cell state among mouse SSCs and progenitors

(A–C) Phosphorylated MAPK (phospho-MAPK) (A), phosphorylated AKT (phospho-AKT) (B), and p-RPS6 (C) levels in isolated seminiferous tubule cells from adult *Id4-Egfp* mice gated for quiescent SSCs (ID4-EGFP^{Bright}/SOX3^{low}/Ki67^{low}, orange), activated SSCs (ID4-EGFP^{Bright}/SOX3^{low}/Ki67^{high}, green), and early progenitors (ID4-EGFP^{Bright}/SOX3^{high}, red) compared with unstained negative control cells (gray). Gating controls are in Figure S3H.

(D) Quantification of flow cytometry from (A)–(C) (n = 3 adult *Id4-Egfp* mice). Dot size, proportion of undifferentiated spermatogonia; color, percentage that are marker positive.

(E) WM-IIF of PLZF (green, spermatogonia), p-RPS6 (red, mTORC1 activity), SOX3 (white, early/late progenitors), and Ki67 (blue, proliferation) in adult C57BL/6 mice.

Arrowhead, quiescent SSCs (PLZF+/SOX3−/Ki67−); circle, early progenitors (PLZF+/SOX3+/Ki67+). Scale bar, 20 μm.

(F) Quantification of p-RPS6 levels in quiescent SSCs (ID4-EGFP^{Bright}/SOX3^{low}/Ki67^{low}), activated SSCs (ID4-EGFP^{Bright}/SOX3^{low}/Ki67^{high}), and early progenitors (ID4-EGFP^{Bright}/SOX3^{high}) in untreated and rapamycin-treated adult *Id4-Egfp* mice (n = 3 adult *Id4-Egfp* mice). Dot size, proportion of undifferentiated spermatogonia; color, percentage marker positive.

(G) Proportion of SSCs (KIT−/PLZF^{low}/SOX3^{low}/RARγ^{low}), early progenitors (KIT−/PLZF^{low}/SOX3^{high}/RARγ^{low}), and late progenitors (KIT−/PLZF^{high}/SOX3^{high}/RARγ^{high}) in untreated and rapamycin-treated adult C57BL/6 mice (see controls in Figure S3J). Data are mean ± SEM. Two-tailed Student's t test (*p < 0.05, **p < 0.01, and ***p < 0.001).

(H) Quantification of flow cytometry analysis of Ki67 levels in untreated (n = 3) and rapamycin-treated (n = 3) adult C57BL/6 mice gated for SSCs (KIT−/PLZF^{low}/SOX3^{low}/RARγ^{low}), early progenitors (KIT−/PLZF^{low}/SOX3^{high}/RARγ^{low}), and late progenitors (KIT−/PLZF^{high}/SOX3^{high}/RARγ^{high}). Gating controls are in Figure S3J. Data are mean ± SEM. Two-tailed Student's t test (*p < 0.05 and **p < 0.01).

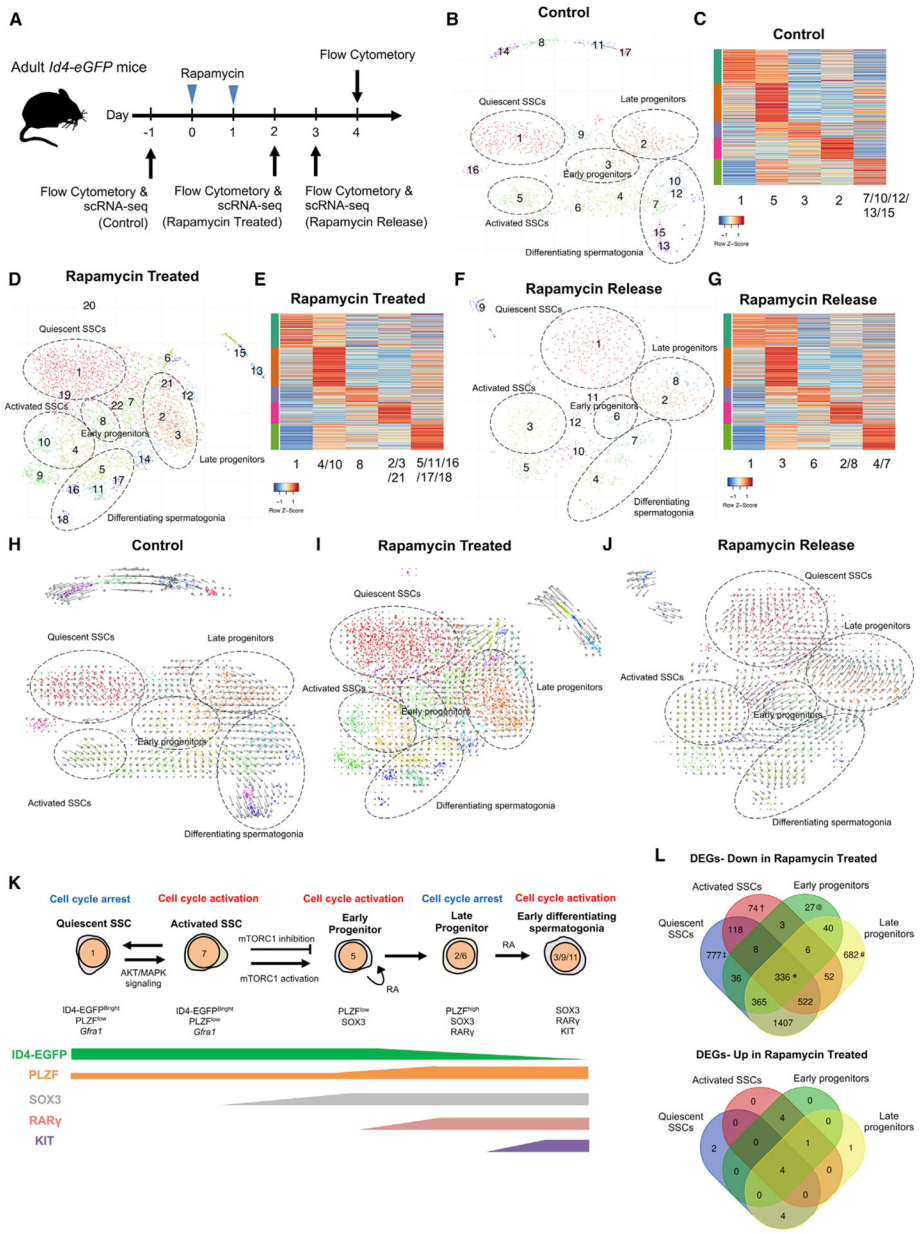

Figure 4. mTORC1 signaling regulates the balance between SSC self-renewal and commitment to spermatogonial differentiation

(A) Experimental design cartoon. Blue arrowheads indicate rapamycin treatments, and black arrows indicate analysis points.

(B–G) RNA velocity clustering of adult ID4-EGFP^{Bright} spermatogonia from (B) untreated control mice, (D) day 2 rapamycin-treated mice, or (F) day 3 rapamycin-release mice (1 day washout of rapamycin). Clusters are color coded and numbered. Dotted ovals denote quiescent SSCs, activated SSC, early progenitors, late progenitors, and differentiating spermatogonia. (C, E, and G) Heatmaps depict cell-type-specific DEGs defined in Figure S1I. (C) Untreated control mice. (E) Day 2 rapamycin-treated mice. (G) Day 3 rapamycin-release mice. See Figure S5.

(H–J) RNA velocity vector fields indicate the observed (dots) and extrapolated future states (arrows) in spermatogonia from (H) control, (I) rapamycin-treated, or (J) rapamycin-release testes.

(K) Model showing MAPK/AKT signaling activation associated with the interconversion between quiescent SSCs and activated SSCs, and an mTORC1-dependent switch promoting a reversible transition from activated SSCs to SOX3^{high}/RARγ^{low} early progenitors. Retinoic acid (RA) enhances the proliferation of early progenitors, and acquisition of a SOX3^{high}/RARγ^{high} late progenitor phenotype coincides with exit from the cell cycle. RA stimulates late progenitors to produce KIT-positive differentiating spermatogonia.

(L) Venn diagram depicting the overlap of downregulated genes (above) and upregulated genes (below) in rapamycin-treated spermatogonial populations. *, DEGs downregulated in all rapamycin-treated spermatogonia; ‡, unique DEGs downregulated in rapamycin-treated quiescent SSCs; †, unique DEGs downregulated in rapamycin-treated activated SSCs; @, unique DEGs downregulated in rapamycin-treated early progenitors; #, unique DEGs downregulated in rapamycin-treated late progenitors.

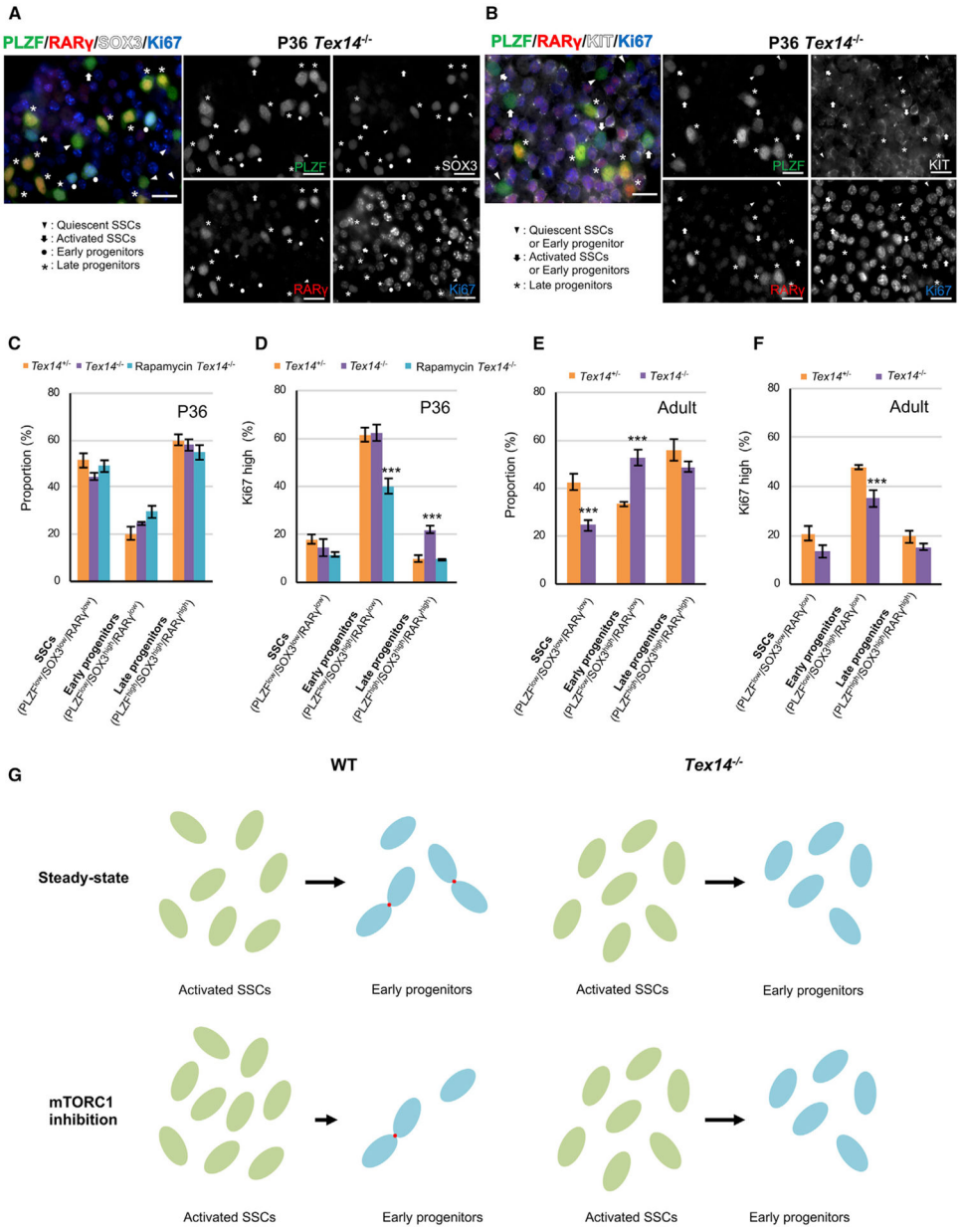

Figure 5. mTORC1 inhibition fails to drive activated SSC accumulation and early progenitor depletion in the absence of intercellular bridges

(A and B) WM-IIF of PLZF (green, spermatogonia), RARγ (red, late progenitors), SOX3 (white, early/late progenitors) or KIT (white, differentiating spermatogonia), and Ki67 (blue, proliferation) in seminiferous tubules from P36 *Tex14*$^{-/-}$ mice. Arrowhead, quiescent SSCs (PLZF+/SOX3−/RARγ/Ki67−) or early progenitors (PLZF+/KIT−/RARγ−/Ki67−); arrow, activated SSCs (PLZF+/SOX3−/RARγ−/Ki67+) or early progenitors (PLZF+/KIT−/RARγ−/Ki67+); circle, early progenitors (PLZF+/SOX3+/RARγ−/Ki67+); asterisk, late progenitors (PLZF+/SOX3+ or KIT−/RARγ+/Ki67−). Scale bar, 20 μm.

(C) Proportion of SSCs (KIT−/PLZF^{low}/SOX3^{low}/RARγ^{low}), early progenitors (KIT−/PLZF^{low}/SOX3^{high}/RARγ^{low}), and late progenitors (KIT−/PLZF^{high}/SOX3^{high}/RARγ^{high}) in seminiferous tubule cells from control (n = 3) and rapamycin-treated (n = 3) *Tex14*$^{-/-}$

mice at P36 (see controls in Figure S3J). Data are mean ± SEM. (D) Ki67 staining intensity in SSCs (KIT−/PLZF^{low}/SOX3^{low}/RARγ^{low}), early progenitors (KIT−/PLZF^{low}/SOX3^{high}/RARγ^{low}), and late progenitors (KIT−/PLZF^{high}/SOX3^{high}/RARγ^{high}) in seminiferous tubule cells from *Tex14*$^{+/−}$, *Tex14*$^{−/−}$, and rapamycin-treated *Tex14*$^{−/−}$ mice (n = 3 each) at P36 (see controls in Figure S3J). Data are mean ± SEM. Two-tailed Student's t test (***p < 0.001).

(E) Proportion of SSCs (KIT−/PLZF^{low}/SOX3^{low}/RARγ^{low}), early progenitors (KIT−/PLZF^{low}/SOX3^{high}/RARγ^{low}), and late progenitors (KIT−/PLZF^{high}/SOX3^{high}/RARγ^{high}) in seminiferous tubule cells from adult control (n = 3) and rapamycin-treated (n = 3) *Tex14*$^{−/−}$ mice (see controls in Figure S3J). Data are mean ± SEM. Two-tailed Student's t test (***p < 0.001).

(F) Ki67 staining intensity in SSCs (KIT−/PLZF^{low}/SOX3^{low}/RARγ^{low}), early progenitors (KIT−/PLZF^{low}/SOX3^{high}/RARγ^{low}), and late progenitors (KIT−/PLZF^{high}/SOX3^{high}/RARγ^{high}) in seminiferous tubule cells from adult (>60 days) control (n = 3) and rapamycin-treated (n = 3) *Tex14*$^{−/−}$ mice (see controls in Figure S3J. Data are mean ± SEM. Two-tailed Student's t test (***p < 0.001).

(G) Model positing that the transition between activated SSCs and clones of early progenitors is dependent upon mTORC1 activity.

KEY RESOURCES TABLE

REAGENT or RESOURCE	SOURCE	IDENTIFIER
Antibodies		
Goat anti-SOX3 antibody (0.8 μg/mL); Figures 2, 3, 5, and S3–S5	R&D Systems	RRID: AB_2239933 Cat# AF2569
Goat anti-c-KIT antibody (4 μg/mL); Figures 5 and S3–S5	R&D Systems	RRID: AB_354750 Cat# AF1356
Mouse anti-PLZF antibody (Clone 2A9; 4 μg/mL); Figures 2, 3, 4, 5, and S3–S5	Active Motif	RRID: AB_213280 Cat# 39988
Rabbit anti-RARγl antibody (Clone D3A4; 4.536 μg/mL); Figures 3, 4, 5, and S3–S5	Cell Signaling Technology	RRID: AB_10998934 Cat# 8965
Rabbit anti-phospho-p44/42 MAPK (Thr202/Tyr204) (0.18 μg/mL); Figure 4	Cell Signaling Technology	RRID: AB_331646 Cat# 9101
Rabbit anti- anti-phospho-pan-AKT (Ser473) (0.354 μg/mL); Figure 4	Cell Signaling Technology	RRID: AB_2315049 Cat# 4060
Rabbit anti-phospho-RPS6 (Ser235/236) antibody (Clone D57.2.2E; 0.118 μg/mL); Figure 4	Cell Signaling Technology	RRID: AB_916156 Cat# 4858
Rat anti-Ki67 (Clone SolA15; 2 μg/mL); Figures 2, 3, 5, S3, and S4	ThermoFisher	RRID: AB_10854564 Cat# 14-5698-82
Biotin anti-mouse CD9 Antibody (Clone MZ3; 1 μg/ml); Figures 2 and 4	Biolegend	RRID: AB_2275863 Cat# 124804
APC-conjugated rat anti-c-KIT (Clone 2B8; 4μg/ml); Figures 3, 5, and S3–S5	Biolegend	RRID: AB_313221 Cat# 105812
APC-conjugated Rat IgG2b kappa Isotype Ctrl Antibody (Clone eB149/10H5; 4μg/ml); Figure S3	ThermoFisher	RRID: AB_470176 Cat# 17-4031-82
Alexa Flour 700-conjugated Rat IgG2b kappa Isotype Ctrl Antibody (Clone RTK4530; 2μg/ml); Figure S3	Biolegend	RRID: AB_493783 Cat# 400628
Biotin Mouse IgG1 K Isotype Control (Clone MOPC-21; 1μg/ml); Figure S3	BD PharMingen	RRID: AB_396089 Cat# 555747
Alexa Flour 700-conjugated rat anti-Ki67 (Clone SolA15; 2μg/ml); Figures 2, 3, 5, and S3–S5	ThermoFisher	RRID: AB_2637480 Cat# 56-5698-82
Alexa Fluor 488 Donkey anti-mouse IgG (2 μg/mL); Figures 2, 3, 5, and S3–S5	ThermoFisher	RRID: AB_141607 Cat# A-21202
Alexa Fluor 488 Donkey anti-goat IgG (2 μg/mL); Figures 2 and S4	ThermoFisher	RRID: AB_2762838 Cat# A-32814
Alexa Fluor 568 Donkey anti-rabbit IgG (4 μg/mL); Figures 2, 3, 5, and S3–S5	ThermoFisher	RRID: AB_2534017 Cat# A-10042
Alexa Fluor 568 Donkey anti-mouse IgG (2 μg/mL); Figures 2 and S4	ThermoFisher	RRID: AB_2534013 Cat# A-10037
Alexa Fluor 405 Donkey anti-rat IgG (8 μg/mL); Figures 2 and S4	Abcam	Cat# ab175670
Alexa Fluor 405 Donkey anti-goat IgG (8 μg/mL); Figures 2, 3, 5, and S3–S5	Abcam	RRID: AB_2313502 Cat# ab175664
Alexa Fluor 568 Donkey anti-rat IgG (4 μg/mL); Figures 2 and S4	Abcam	RRID: AB_2636887 Cat# ab175475
Alexa Fluor 647 Donkey anti-rat IgG (8 μg/mL); Figures 3, 5, and S3–S5	Abcam	RRID: AB_2813835 Cat# ab150155
Chemicals, peptides, and recombinant proteins		
Lectin PNA From Arachis hypogaea (peanut), Alexa Fluor 647 Conjugate (4 μg/mL); Figure 2	Invitrogen	Cat# L32460
Streptavidin-APC (0.08mg/ml); Figures 2, 4, and 5	Biolegend	Cat# 405207
all-*trans*RA (100 μL injections of 7.5 mg/mL)	Sigma-Aldrich	Cat# R2625
WIN18,446 (100 μL injections of 20 mg/mL)	Santa Cruz Biotechnology	Cat# sc-295819A
Rapamycin (100 μL injections of 0.8 mg/mL)	Biotang Inc.	Cat# 53123-88-9
Critical commercial assays		

REAGENT or RESOURCE	SOURCE	IDENTIFIER
Chromium Single Cell 3' v3 Reagent Kits & Chip Kits	10x Genomics	Cat# PN-1000075
Deposited data		
Raw and analyzed 10x Genomics scRNA-seq datasets from Adult ID4-EGFP-bright spermatogonia from Control, Rapamycin-treated and Rapamycin-release testes	This paper	GEO: GSE152930
Raw and analyzed Adult Mouse spermatogenic cell 10x Genomics scRNA-seq data	Hermann et al., 2018	GEO: GSE109033
Raw and analyzed Adult Mouse spermatogonia 10x Genomics scRNA-seq data	La et al., 2018b	GEO: GSE107256
Custom Mouse reference dataset GRCm38 (mm10) containing EGFP cDNA required for Cell Ranger, v3.1.0	This paper	Mendeley Data: https://doi.org/10.17632/xzk2zyymxy.1
Experimental models: organisms/strains		
Mouse: C57BL/6J	The Jackson Laboratory	RRID:IMSR_JAX:000664
Mouse: B6-Cg-*Id4-Egfp(LT-11)*	Chan et al., 2014	N/A
Mouse: B6;129S-Tex14	Greenbaum et al., 2006	RRID:MGI:3624029
Software and algorithms		
FlowJo v9	FlowJo, LLC	https://www.fiowjo.com/solutions/fiowjo/downloads/v9
AxioVision 4.8.2	Zeiss	https://www.micro-shop.zeiss.com/en/us/system/software+axiovision-axiovision+program-software/10221/
velocyto.R (v0.6)	Svensson and Pachter, 2018; La Manno et al., 2018	https://github.com/velocyto-team/velocyto.R
edgeR (v3.22.3)	Robinson et al., 2010	https://bioconductor.org/packages/release/bioc/html/edgeR.html
Cell cycle analysis	Whitfield et al., 2002	http://jdblischak.github.io/singleCellSeq/analysis
TCC (Deseq2) (v1.20.1)	Sun et al., 2013	https://bioc.ism.ac.jp/packages/3.3/bioc/html/TCC.html
Cell Ranger v3.1.0	10x Genomics	https://support.10xgenomics.com/single-cell-gene-expression/software/downloads/latest
ggplot2 (v3.2.1)	Wickham, 2016	https://github.com/tidyverse/ggplot2/releases
gplot (v3.0.1.1)	Github	https://github.com/talgalili/gplots